TURBULENCE IN WAVING WHEAT

II. Structure of Momentum Transfer

J. J. FINNIGAN

Division of Environmental Mechanics, CSIRO, Canberra, Australia

(Received 10 November, 1978)

Abstract. The intermittent features of the turbulent velocity field within a wheat canopy were investigated by conditional sampling techniques and short-period space-time correlations. The velocity and shear-stress profiles had qualitatively quite different forms during periods of high and low winds. Analysis of the relative importance of shear-stress contributions from different quadrants of the uw plane revealed the dominant role of gusts in penetrating the canopy and transferring momentum to it from the boundary layer above. Short-period space-time correlations of velocity indicated that over a significant fraction of the time, periodic velocity fluctuations pervaded the canopy-air layer. It is surmised that while this has only a secondary effect on momentum transfer, it may be of overriding importance in heat and mass transport.

Notation

x streamwise co-ordinate positive downwind
y cross-stream co-ordinate
z vertical co-ordinate, positive upwards
$\tilde{u}$ instantaneous streamwise velocity
$\tilde{v}$ instantaneous cross-stream velocity
$\tilde{w}$ instantaneous vertical velocity
$\tilde{u} = U + u; \quad U = \bar{\tilde{u}}; \quad \bar{u} = 0$
$\tilde{w} = W + w; \quad W = \bar{\tilde{w}}; \quad \bar{w} = 0$
$\tilde{v} = V + v; \quad V = \bar{\tilde{v}}; \quad \bar{v} = 0$
$\tilde{p}$ instantaneous pressure
$\tilde{p} = P + p; \quad P = \bar{\tilde{p}}; \quad \bar{p} = 0$

$$\bar{q} = \lim_{T \to \infty} \frac{1}{T} \int_0^T q(t)\, \mathrm{d}t$$

$\bar{}$ denotes long time average
$=$ denotes short time average
$\hat{}$ denotes conditional average
subscript $_R$ denotes reference wire ($z = 2.0$ m)
Other symbols are defined as they are encountered in the text.

1. Introduction

This paper is the second part of an investigation into the turbulence structure of a wheat canopy, conducted with the primary aim of establishing those features of momentum transfer which are masked by long time averages. A body of data, collected in smooth- and rough-wall turbulent boundary layers, has emphasized the essential intermittency in time and space of Reynolds stress (for a review of some of these results see Willmarth, 1975). The results of Dorman and Mollo-Christensen (1973), obtained over an open water surface, showed that intermittent periods of

Boundary-Layer Meteorology **16** (1979) 213–236. 0006-8314/79/0162-0213$03.60

high momentum transfer were accompanied by instantaneous velocity profiles very different from the mean. At the same time, a few isolated results from field experiments in plant canopies (Allen, 1968; Isobe, 1972) have suggested that air motions with length scales much larger than those typical of the canopy might make important contributions to the velocity field.

Most mathematical models of canopy flow have, however, attempted to relate the canopy geometry and time-averaged momentum absorption by a process of continuous diffusion by turbulent eddies, expressed as a flux-gradient relationship and characterized by a single-valued diffusivity or mixing length (see, for example, Cowan, 1968; Thom, 1972). This approach has been criticized on general theoretical grounds by Corrsin (1974); it has also become apparent that it is inadequate to account for observations in many simple canopy-flow situations (Shaw, 1977). It is hoped in this paper to determine the degree of uniformity (or otherwise) of momentum transfer to and within the canopy, in order to test the basic premise of the conventional approach.

In the first part of this investigation (Finnigan, 1979), hereafter referred to as 'Part I', results were analyzed in the conventional manner: time-average, single-point statistics and spectra of the turbulent velocity and surface pressure were presented. The features of the velocity spectra were interpreted in terms of the organized wave motion or 'honami', so prominent in cereal canopies on windy days. It was established that the honami waves were records of the passage of gusts of air with high streamwise momentum, which sweep down to the surface from an outer part of the boundary layer, bending over a series of stalks in their downwind passage. These stalks then spring back and vibrate at their natural frequency, but the small but smoothly varying phase difference between adjacent stalks gives the impression of waves moving through the canopy.

The areas of coherently waving stalks impress a velocity wave upon the air moving through the top of the canopy and the waving frequencies form prominent peaks in the velocity spectra. At the top of the canopy, these peaks are seen to be identical to the waving frequency but move to lower frequencies as one descends into the canopy and higher frequencies as one rises above it. This height dependence of the frequency peaks is ascribed to a combination of a Doppler effect, as regions of fluid containing propagating velocity waves are accelerated past the fixed hot wire, and distortion of the wavelength of the velocity waves by rapid shear of these same regions. For a more detailed discussion of these observations see Part I.

The errors in hot-wire measurements, unavoidable in high intensity turbulence, were shown to be mitigated to some extent in the present experiment by the strong positive skewness of streamwise velocity within the canopy.

2. Experimental Site and Instrumentation

The measurements were made in a uniform crop of wheat, 1.25 m high, at the CSIRO Ginninderra Experiment Station, Canberra, Australia between 9 and 18

December 1976. The primary sensors were single and X-wire anemometer probes mounted on damped wind vanes on a vertical mast. The single wire was fixed at a height of 2 m to provide a reference signal, while the X wire could be moved vertically to obtain profiles. Supplementary instrumentation included a pressure sensor arranged to record pressure at the ground surface, miniature strain gauges glued to wheat stalks to measure their waving directly, and an 8-mm movie camera used to record the waving motion of the field. A description of the instrumentation and field site can be found in Part I.

3. Results and Discussion

The results described in the next three sections were obtained from 5-min records of sensor output at each height. Data were recorded on an analogue tape recorder after first being low-pass filtered at 250 Hz by 4-pole filters with a Butterworth response. The signals were subsequently digitized and linearized using predetermined calibration data on a Digital Equipment Corp. PDP 11/40 computer. Spectra were obtained digitally using a Fast Fourier Transform routine, the time series being tapered before transformation with a 'Hanning Window'. Analysis of the possible aerodynamic mean pressure gradients resulting from inhomogeneities in the site, revealed that the time mean measurements could be interpreted in an essentially one-dimensional framework.

Details of the particular experimental conditions pertaining to each run can be found in Table I. Because of the considerable computing time involved in analyzing

TABLE I
Summary of experimental conditions

Date	Profile No.	Sensors operating	z^* m	U m s^{-1}	U_R m s^{-1}
9/12/76	R1	X wire only	1.55	4.035	—
			1.25	4.096	—
			0.75	1.588	—
			0.35	1.475	—
10/12/76	R2	X wire and reference wire	1.00	1.774	3.07
			0.70	1.18	2.633
			1.50	3.368	4.025
			0.40	1.001	3.575
			1.95	3.235	3.043
			0.10	0.891	3.208
14/12/76	R4	X wire and reference wire	0.4	1.301	5.562
			0.7	1.687	5.192
			1.0	2.090	7.404
			1.3	3.63	8.805
18/12/76	R5	X wire, reference wire, pressure sensor, strain gauges	1.4	5.272	6.229
			1.2	4.670	6.293

* z values are given in the order in which profile was measured.

the data by conditional methods, only the results of Run R2 have been completely processed. However, sufficient spot checks were done on the rest of the data to support the conclusions presented here. The weather conditions at the field site for four of the runs are presented in Table II.

TABLE II
Meteorological data from Ginninderra Field Site. Average quantities are for 24-h period

Date	Wet- and dry-bulb temperatures at 9 a.m. E.S.T.		Maximum and minimum temperatures		Wind run	Pan evaporation
	Dry °C	Wet °C	Max. °C	Min. °C	km	mm H_2O
9/12/78	17.0	15.0	28.0	7.0	129.8	6.4
10/12/78	16.5	15.0	30.0	9.5	167.2	6.2
14/12/78	18.5	11.4	22.2	6.0	151.6	8.0
18/12/78	16.0	11.0	19.5	2.5	125.4	4.0

3.1. Conditionally sampled mean profiles

Typical time traces of the streamwise velocity, $\tilde{u}$, vertical velocity, $\tilde{w}$, and shear stress, $-\overline{\tilde{u}\tilde{w}}$, at various heights in the canopy, together with the simultaneous record of streamwise velocity at $z = 2$ m, $\tilde{u}_R$, are shown in Figure 1. It is immediately obvious that as one descends into the foliage, the turbulent signal begins to acquire an intermittent character until at $z = 0.4$ and 0.1 m, the trace is reminiscent of the outer wake region of a turbulent boundary layer, with periods of strong turbulence separated by quiescent periods. It can be seen that periods of strong turbulence within the canopy are associated with higher than average velocity above the canopy. In an attempt to quantify this relationship, the turbulence statistics were conditionally sampled in the following way. An indicator function, $I(\tilde{u}_R)$, was defined such that

$$I = 1; \quad 2\ \mathrm{m\,s^{-1}} > \tilde{u}_R \geq 0$$

$$I = 2; \quad 3\ \mathrm{m\,s^{-1}} > \tilde{u}_R \geq 2\ \mathrm{m\,s^{-1}}$$

$$I = 3; \quad 4\ \mathrm{m\,s^{-1}} > \tilde{u}_R \geq 3\ \mathrm{m\,s^{-1}}$$

$$I = 4; \quad 5\ \mathrm{m\,s^{-1}} > \tilde{u}_R \geq 4\ \mathrm{m\,s^{-1}}$$

$$I = 5; \quad \tilde{u}_R \geq 5\ \mathrm{m\,s^{-1}}.$$

The conditional average of the turbulence moment of interest, $\hat{\mu}(I)$, (where $\hat{}$ denotes a conditional average, $\bar{}$ a normal average) within the canopy was then computed according to the value of the indicator function such that

$$\hat{\mu}(I) = \frac{1}{m(I)} \sum_{j=1}^{n} \mu_j \delta(I - I_j)$$

where n is the number of digitized values of μ, μ_j and I_j being the jth values of μ and

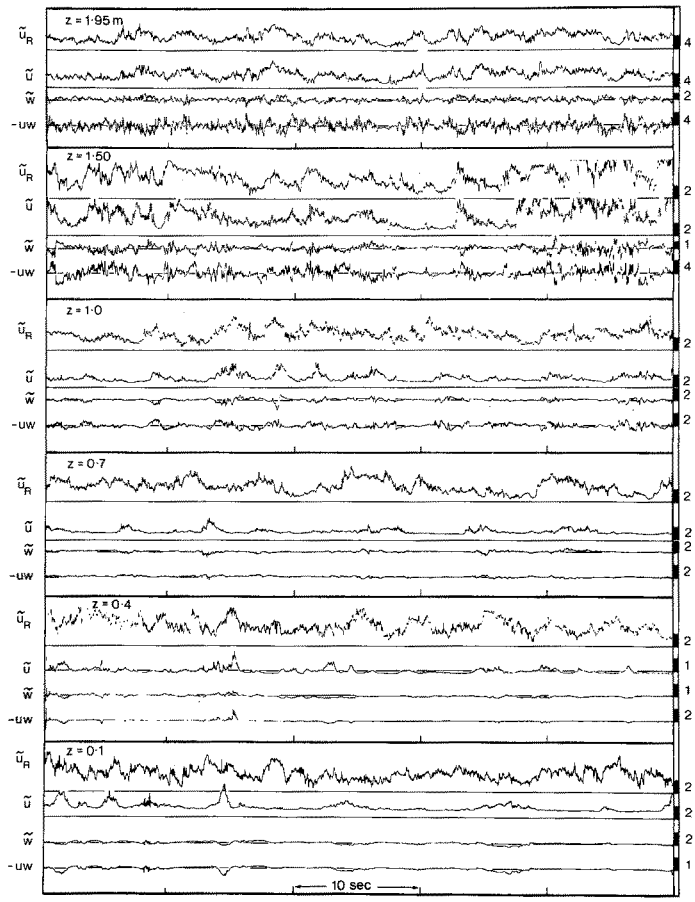

Fig. 1. Computer plots of typical sections of $\tilde{u}_R$, $\tilde{u}$, $\tilde{w}$ (m s^{-1}) and $-uw$ (m^2 s^{-2}) *vs.* time from R2 at various heights, z. The large amplitude fluctuations were truncated by the plotter. This does not imply that the measured signals were truncated.

I, respectively.

$$\delta(I - I_j) = \begin{cases} 1 & \text{if} \quad I_j = I \\ 0 & \text{if} \quad I_j \neq I \end{cases}$$

and $m(I)$ is the number of times $I = I_j$. The conditional sampling process is shown schematically in Figure 2.

The averages were then normalized using the central value of the reference velocity as follows:

$\hat{M}(1)$ normalized with 1 m s^{-1}
$\hat{M}(2)$ normalized with 2.5 m s^{-1}
$\hat{M}(3)$ normalized with 3.5 m s^{-1}
$\hat{M}(4)$ normalized with 4.5 m s^{-1}
$\hat{M}(5)$ normalized with 5.5 m s^{-1}.

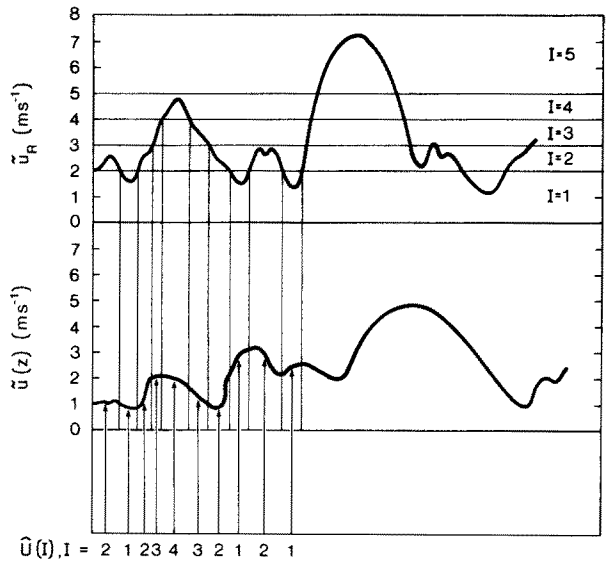

Fig. 2. Diagram of the conditional sampling process forming $\hat{U}(I)$.

The final non-dimensional moments are assumed to indicate the appearance of the moment field if the conditions appropriate to each average occurred all the time. The author realizes that the effect of a change in velocity at 2 m will not be reflected instantly within the canopy but felt that to impose some height dependent time delay, so that averages at z depended upon the value of I some time earlier, was equivalent to an implicit assumption of a propagation mechanism.

Reference to Figure 11, where the variation with height of the time delay of peak correlation between u_R and $u(z)$ is plotted, reveals that the time taken for a change in velocity at $z = 2.0$ m to be felt at $z = 0.10$ m was about 1.40 s, so a compromise was reached by smoothing the relevant signals with a 2-s moving average before the conditional sampling operation.

The mean velocity profiles appropriate to $\tilde{u}_R < 2$ m s^{-1} and $5 > \tilde{u}_R \geq 4$ m s^{-1} are plotted in Figure 3a; the long time average profile U/U_R is included for comparison. Within the upper 50% of the canopy, the shapes of the two conditionally averaged profiles are qualitatively different; stronger winds or gusts appear able to penetrate much better into the foliage and the strong-wind profile exhibits much stronger shear in the upper canopy, presumably a result of the stronger absorption of momentum during times of higher wind by the aerodynamic drag of the foliage which increases as $\tilde{u}^2$. The similarity between the strong-wind profile and the time mean profile suggests that the (relatively infrequent) periods when $\tilde{u}_R$ is between 4 and 5 m s^{-1} have a dominant effect on the shape of the long time mean. The relative frequency of occurrence of a given value of I is presented in Figure 3b. The histogram is an average over the whole profile and allows the relative importance of the different wind regimes to be assessed. Some caution is needed in interpreting these profiles. It

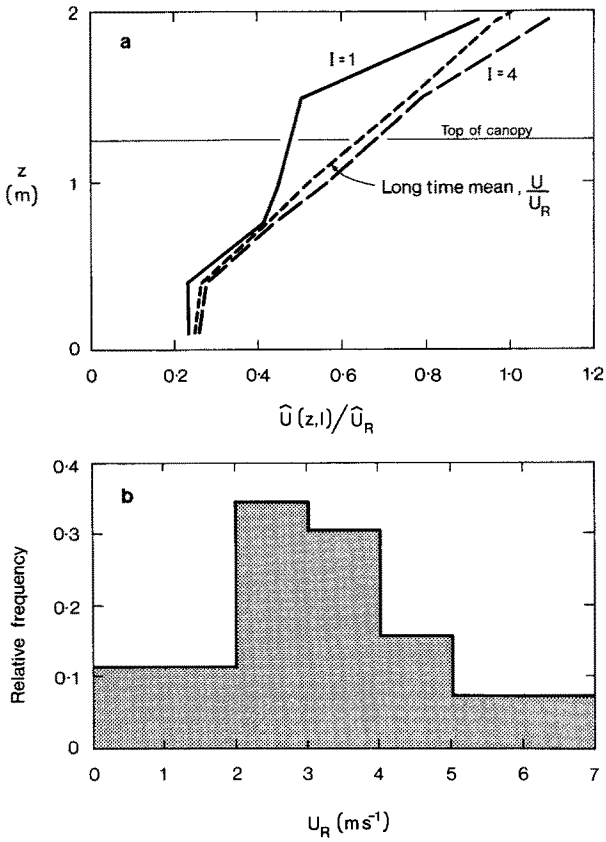

Fig. 3. (a) Normalized conditionally sampled mean velocity, $\hat{U}(z, I)/\hat{U}_R$, *vs.* height, z. (b) Relative frequency of occurrence of a given value of I.

should be realized that profiles obtained by this conditional process are no more representative of instantaneous velocity profiles than is the convential long time mean.

The conditionally averaged shear-stress profiles of Figure 4 appear to be more sensitive to I than are the velocity profiles. They are presented as curves of $\hat{u}_*[=(-\widehat{uw})^{1/2}]$ normalized as before with the appropriate $\hat{U}_R$; the long time mean profile u_*/U_R is included for comparison. It is apparent that, as with the velocity profile, the form of the shear-stress profile is qualitatively quite different during periods of low and high wind. $\hat{u}_*/\hat{U}$ at the top of the canopy for $\tilde{u}_R > 5$ m s^{-1} is about 3 times $\hat{u}_*/\hat{U}$ for $\tilde{u}_R < 2$ m s^{-1}. The mean profile, at least to 1.5 m, appears to coincide with $\hat{u}_*/\hat{U}_R$ for $\tilde{u}_R > 5$ m s^{-1}, suggesting that the dominant contribution to the shear-stress profile comes from times of high wind.

To appreciate the intermittent nature of the momentum transfer, however, it is necessary to consider the fraction of the total time that the indicator function dwelt at its various values. This information has been combined with the conditional average

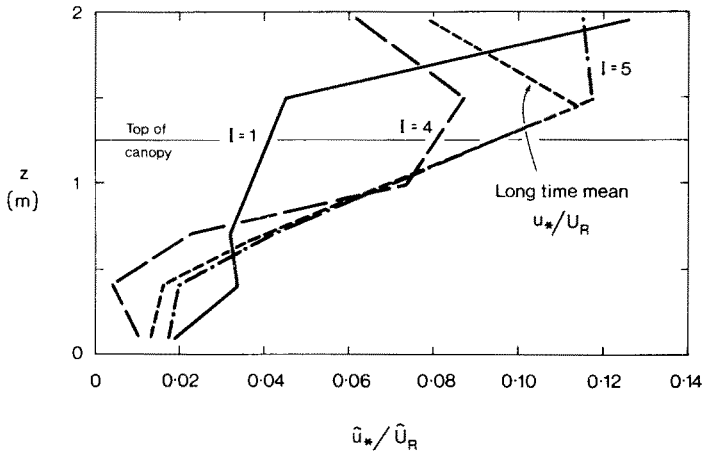

Fig. 4. Normalized conditionally sampled friction velocity, $\hat{u}_*/\hat{U}_R$, *vs.* height, z.

to give a measure of the relative importance of contributions to $\overline{uw}$ from each wind regime. In Figure 5, the fractional contribution to total shear stress for a given indicator function value, divided by the fraction of the total time that the quantity I had that value, is plotted against height (i.e., $[\widehat{uw}(I)/\overline{uw}]/[m(I)/n]$ *vs.* z). Although some points are equivocal (due probably to not having long enough averaging times to attain proper statistical confidence for some infrequent contributions), it is obvious that a large fraction of the total momentum is transferred during times when $\hat{u}_R$ exceeds 5 m s^{-1}, but that these periods are relatively short lived.

These observations suggest an alternative explanation for the commonly observed dependence upon mean wind speed of the total drag coefficient or any other

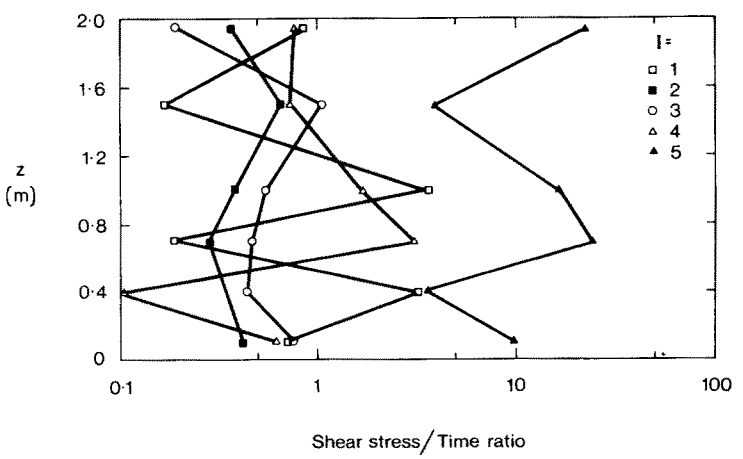

Fig. 5. Fractional contribution to shear stress of each conditional average $\hat{u}_*(I)$ to u_* in a given range of $\hat{U}_R$, divided by fraction of total time in that range.

parameter of a tall cereal crop which is a function of mean momentum absorption, such as the roughness length, z_0, or the zero-plane displacement of the logarithmic wind profile (see Inoue *et al.*, 1975; Maki, 1975a, b). A decreasing total drag coefficient, C (where $C = -2\overline{uw}/U^2$ at some height above the crop), with increasing mean wind speed is usually ascribed to streamlining of the crop as it bends before the wind. These observations, however, may well be a result of an inappropriate normalizing function, U^2, for the drag regime in the canopy. In light winds, the present results indicate that few gusts would penetrate the canopy and winds would be low in the lower part of the foliage. The aerodynamic regime at these levels would then be primarily laminar. Taking a cylinder as representing a typical canopy element, at Reynolds numbers lower than about 10^3 (corresponding to a stalk diameter of 0.01 m and a wind speed of 1.5 m s^{-1}, typical of lower canopies in light winds) the drag coefficient based on cylinder diameter and U^2 rises rapidly as U decreases (Hoerner, 1965). This is a result of using incorrect scaling criteria for the low Reynolds-number regime; wetted surface area and $U^{3/2}$ are the correct scales. It has been pointed out in Part I that the period between gusts decreases with U_R so that the total time that a given depth of the canopy contributes to momentum absorption primarily through laminar skin friction decreases rapidly as U_R increases. Contributions to drag in the lower canopy from form drag during intermittent periods of high wind would outweigh the laminar contribution, so that the drag coefficient, C, of the whole canopy would decrease as the mean velocity increased.

3.2. Quadrant representation of shear stress

The results presented in the preceding section indicate that momentum transfer is an intermittent process, occurring at times when gusts penetrate into the canopy; the velocity profile then differs from its form in light winds. To proceed, further information about the instantaneous features of the velocity field which contribute to the average shear stress, $-\overline{uw}$, is needed. This can be obtained by sorting the contributions to $\overline{uw}$ into four parts depending upon the quadrant of the uw plane in which the correlation occurred (Lu and Willmarth, 1973). The four conditional averages are defined as:

$\widehat{uw}_1$ when $u > 0$, $w > 0$: outward interaction

$\widehat{uw}_2$ when $u > 0$, $w < 0$: gust or sweep

$\widehat{uw}_3$ when $u < 0$, $w < 0$: inward interaction

$\widehat{uw}_4$ when $u < 0$, $w > 0$: burst.

$\widehat{uw}_1$ and $\widehat{uw}_3$ make positive contributions to the mean, and $\widehat{uw}_2$ and $\widehat{uw}_4$ negative contributions. It is useful to define normalized versions of these conditional averages so $RS_n = \widehat{uw}_n/|\overline{uw}|$ and $\sum_{n=1}^{4} RS_n = -1$.

In Figure 6, the normalized averages, RS_n, are plotted against height for three different profiles, R2, R4 and R5. Within and above the canopy, the resultant $\overline{uw}$ is the relatively small difference between the large negative and positive contributions

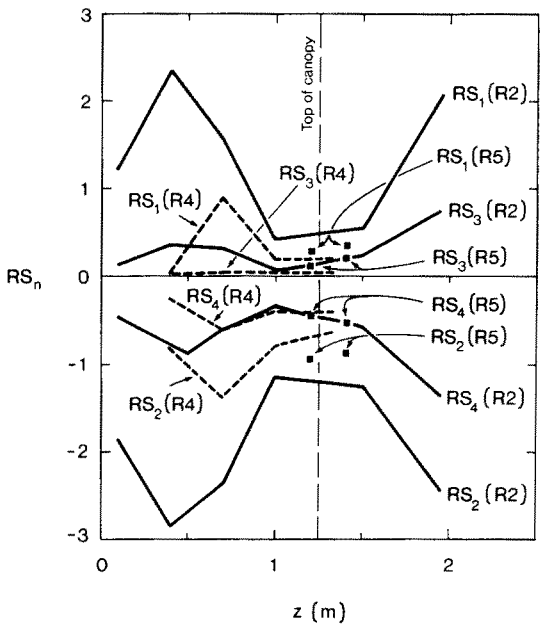

Fig. 6. Normalized contribution to $\overline{uw}$ from each quadrant, RS_n, versus height, z. Data from runs R2, R4, R5.

from sweeps and outward interactions, respectively. It has been established that in smooth-wall turbulent boundary layers in the laboratory, the average frequency of gust arrival at the surface can be scaled with the mean velocity and the boundary-layer thickness (Lu and Willmarth, 1973). In Part I, results were presented which suggested similar behaviour over the wheat canopy, at least over the Reynolds-number range of this experiment. The large values of RS_1 and RS_2 from R2 reflect the increased intermittency of Reynolds stress arrival which is associated with a lower mean wind speed than in R4 and R5. Relatively few gusts are available to penetrate to the middle reaches of the canopy and their contributions to the stress budget are several times the mean.

Within the canopy, bursts and inward interactions are negligible; but above the canopy, bursts start to increase in importance until at $z = 1.95$ m, $RS_4 \simeq RS_1$. There are not many published results with which these observations can be directly compared. Only Nakagawa and Nezu (1977) have analyzed Reynolds stress over a rough wall using the quadrant representation. Their results, obtained in an open channel flow, show that as the wall is approached, sweeps take over from bursts as the principal mechanism of momentum transfer and that this effect is more pronounced as the surface roughness increases. In the outer 90% of the boundary layer, bursts outweigh sweeps and both are two or three times as large as contributions from the other two quadrants. Grass (1971) deduced this same behaviour from flow visualization in an open rough-wall channel flow; however, both these experiments were conducted at considerably lower Reynolds numbers than in the present study.

The only work at comparable Reynolds numbers is that of Weiss and Allen (1976), who measured the flux angle distribution of momentum $\phi(\alpha)$ above vine rows, where $\phi(\alpha)$ was defined by the relation

$$\frac{1}{T}\int_{-\pi}^{\pi}\phi(\alpha)\,\mathrm{d}\alpha = -\overline{uw},$$

T being the averaging time and $\alpha = \tan^{-1} w/u$ so that

$$RS_1 = \frac{1}{|\overline{uw}|}\frac{1}{T}\int_{0}^{\pi/2}\phi(\alpha)\,\mathrm{d}\alpha;$$

$$RS_2 = \frac{1}{|\overline{uw}|}\frac{1}{T}\int_{0}^{-\pi/2}\phi(\alpha)\,\mathrm{d}\alpha;$$

$$RS_3 = \frac{1}{|\overline{uw}|}\frac{1}{T}\int_{-\pi/2}^{\pi}\phi(\alpha)\,\mathrm{d}\alpha;$$

$$RS_4 = \frac{1}{|\overline{uw}|}\frac{1}{T}\int_{\pi/2}^{\pi}\phi(\alpha)\,\mathrm{d}\alpha.$$

Their measurements were made at heights of 6.4 and 4.1 m above the ground with vine rows 2 m high. Figure 7, which is redrawn from Weiss and Allen (1976), shows the relative intensity of gusts (RS_2) compared to bursts (RS_4) over their surface.

Both sweeps and bursts are manifestations of the large eddies or 'coherent structures' which are the characteristic feature of turbulent boundary layers. In a very simplified picture, these eddies have the general form of spanwise vortices (but are of limited spanwise extent) with a rotation in the sense of a ball rolling downwind along the surface when viewed from a co-ordinate system moving with the eddy. Sweeps or gusts are identified with the downwind face of the eddy which carries high momentum fluid from the outer part of the boundary layer to the surface (Brown and Thomas, 1976). As the rearward face of the eddy moves upwards, it lifts the highly sheared layer of fluid close to the surface into the outer part of the layer, causing intense, localized 'bursts' of turbulence (Laufer, 1972). (This idealized description only applies to the plane of symmetry of these complex structures, which in reality probably exhibit some features of the 'Double Roller' eddy proposed by Townsend, 1976.)

In Part I it was shown that when a gust arrives at the canopy surface it initiates a period of strong waving in the stalks and that the stalks' displacement in the x

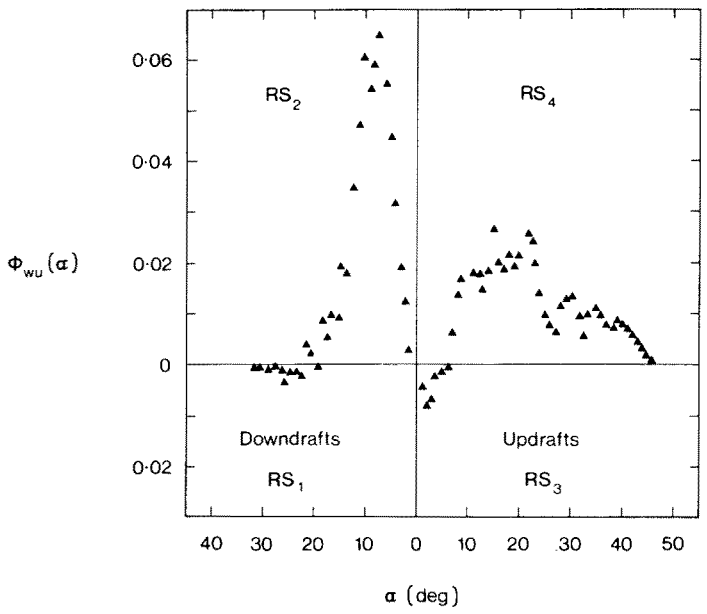

Fig. 7. Flux angle distribution of momentum, $\phi_{wu}(\alpha)$, over vine rows, redrawn from Weiss and Allen (1974).

direction, ξ, can be described by a travelling wave of the form

$$\xi = \xi_0 \exp 2\pi i\left(\frac{x}{\lambda} - ft\right), \tag{1}$$

where ξ_0 is the amplitude of the waving, λ the wavelength and f the frequency. The phase velocity of the waves, $\theta(=\lambda f)$, is a record of the velocity of the gust as it passed over the surface. On average, θ was about 1.8 times the mean velocity at the top of the canopy. The motion of the stalks in the wake of a gust modulates the airstream in the upper canopy through the medium of aerodynamic drag, and continuity ensures that fluctuations in streamwise velocity are accompanied by $\tilde{w}$ fluctuations so that a transverse wavelike motion is imposed upon the background turbulent paths of the fluid particles.

It is suggested that this wavelike particle path is the reason for large values of RS_2 and RS_1 in the mid-canopy, since periods of strong waving are associated with larger than average streamwise velocity (see Part I) and w at a point is alternately positive and negative as the wave progresses. The absence of an important contribution by outward interactions in the measurements of Weiss and Allen (Figure 7) reinforces this argument.

More information about the relative intermittency of the various contributions, RS_n, can be obtained by adding a fifth region, the 'hole', to the quadrant representation of shear stress. The hole is delimited by the curves $|uw| = \text{constant}$, where $|uw| = H|\overline{uw}|$. The five regions are defined in Figure 8. With this scheme, we can

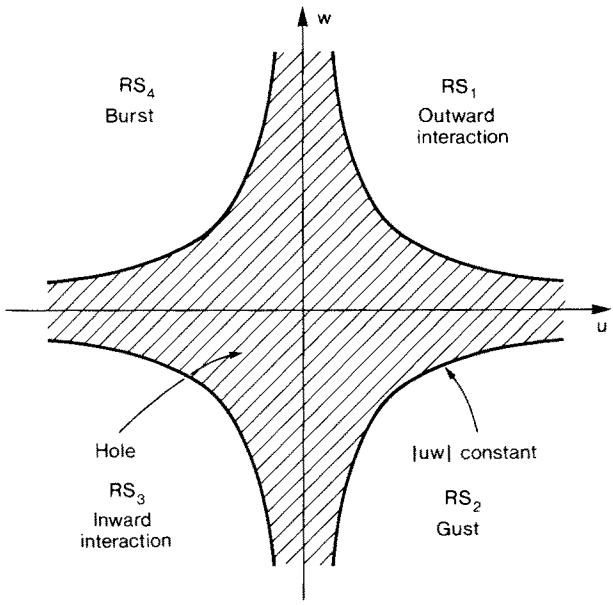

Fig. 8. Schematic drawing of the five regions of the 'quadrant and hole' representation in uw space.

extract large contributions to $\overline{uw}$ from each quadrant by defining $\widehat{uw}_i^*$ such that

$$\widehat{uw}_i^*(H) = \frac{1}{m} \sum_{k=1}^{m} \widehat{uw}_{ik} \cdot Y(k, H)$$

where $\widehat{uw}_{ik}$ is the kth member of the m digitized values of $\widehat{uw}_i$ in the ith quadrant and

$$Y(k, H) = \begin{cases} 1 & \text{if } |\widehat{uw}_{ik}| \geq H \cdot |\overline{uw}| \\ 0 & \text{if } |\widehat{uw}_{ik}| < H \cdot |\overline{uw}| \,. \end{cases}$$

In Figure 9, the dependence of $\widehat{uw}_i^*$ upon H for each quadrant is plotted for each height in the R2 profile. At the top of and above the canopy, the contributions $RS_i^* = \widehat{uw}_i^*/|\overline{uw}|$ for the two most important quadrants, sweeps and outward interactions, decrease relatively rapidly with changing H, $RS_i^*/RS_i|_{i=1,2}$ being less than 0.1 by the time $H = 20$. Within the canopy, however, $RS_i^*/RS_i|_{i=1,2}$ is still about 0.4 at $H = 40$. In other words, throughout and just above the canopy, contributions to shear stress are generally much greater than the mean but this feature is emphasized deep within the canopy by the more infrequent penetration of gusts to these regions. The corresponding dependence of RS_3^* and RS_4^* upon H, plotted in Figure 9, shows that these events make their contributions to the shear-stress budget at only a few multiples of $|\overline{uw}|$.

3.3. Correlations

The obvious way to investigate the dependence of the velocity within the canopy

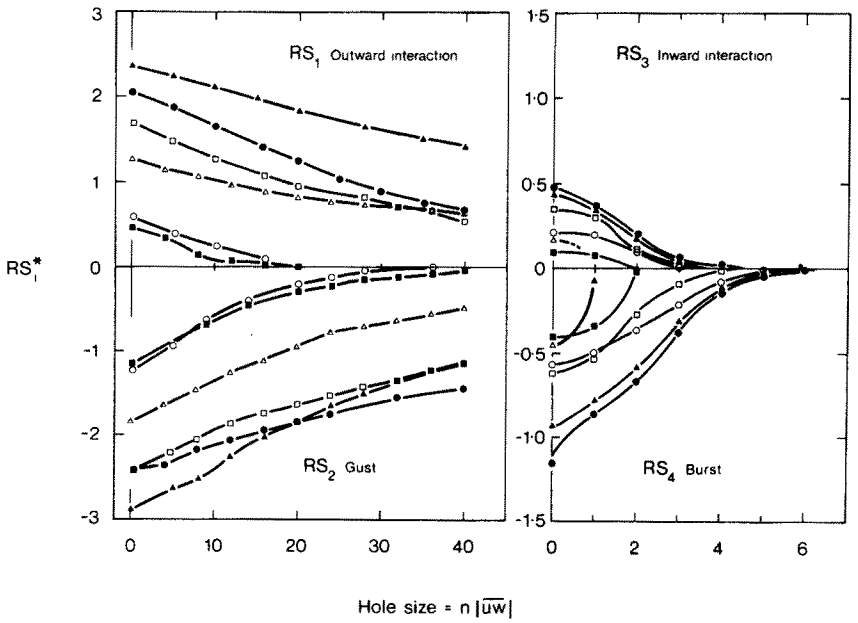

Fig. 9. Normalized contributions of RS_i^* to $\overline{uw}$ *vs.* hole size, $H|\overline{uw}|$, at various heights, z (m): ● 1.95, ○ 1.5, ■ 1.0, □ 0.7, ▲ 0.4, △ 0.1.

upon that above is to compute the space–time correlation coefficient, $R_{uu_R}(z, \tau)$ where

$$R_{uu_R} = [\overline{u(z, t-\tau/2) \cdot u_R(t+\tau/2)}]/[\overline{u^2}(z, t-\tau/2) \cdot \overline{u_R^2}(t+\tau/2)]^{1/2} . \quad (2)$$

Curves of $R_{uu_R}(z, \tau)$ against time delay τ are presented in Figure 10 for profile R2. The correlation diminishes from a value of 0.8 at a vertical separation of 0.05 m to 0.16 at a separation of 1.90 m. Figure 11 presents the time delay of the peak of maximum correlation as a function of height, $\tau_p(z)$. With the exception of that at 0.7 m, the points fall upon a smooth curve. If we define the vertical convection velocity of the peak correlation as $(\mathrm{d}\tau_p/\mathrm{d}z)^{-1}$, the speed with which a streamwise velocity fluctuation at $z = 2$ m propagates towards the surface, we see that the convection velocity decreases as one descends into the canopy, to become approximately constant below $z = 1.0$ m. The curve of Figure 11 can be compared with similar data obtained in a rigid wind-tunnel model canopy by Seginer and Mulhearn (1977). They suggest that their curve of time delay against separation approaches asymptotically the level of zero-plane displacement within the canopy, although it is not clear why this should be so. In the light of the present results, it seems more likely that their curve should be extrapolated linearly to the level, $z = 0$.

In Part I, it was observed that the patches of coherent waving (honami) which appear in the canopy in the wake of gusts are randomly distributed in space and time. The long time averaging involved in computing the correlation R_{uu_R} will tend to smooth out the contributions of this coherent motion.

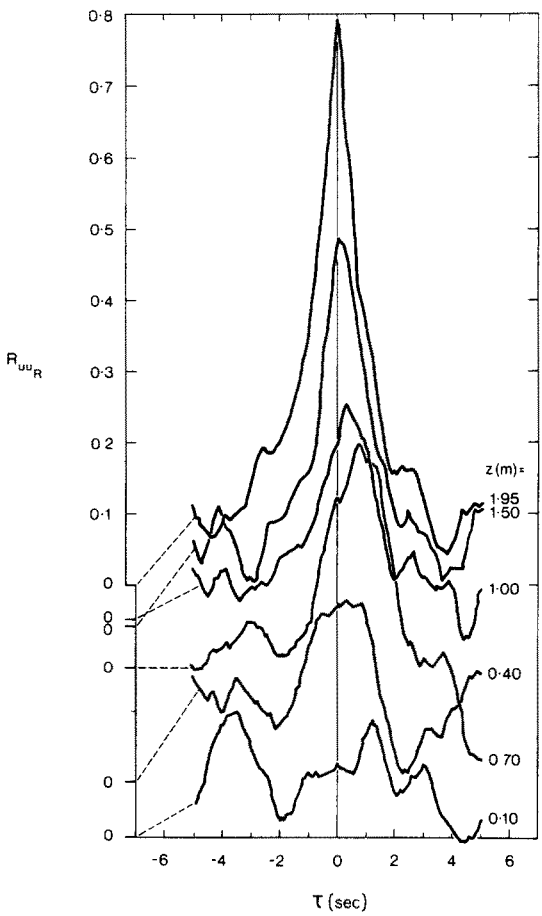

Fig. 10. Long period space-time correlations R_{uu_R} of u_R and u from R2.

Accordingly a series of short period space-time correlations was calculated for successive 10-s intervals of the various time traces of R2 and R5. The short period time-space correlation is defined as

$$R^*_{uu_R}(z,\tau)=[\overline{\overline{u'(t+\tau/2)\cdot u'_R(t-\tau/2)}}]/[\overline{\overline{(u')^2}}(t+\tau/2)\cdot\overline{\overline{(u'_R)^2}}(t-\tau/2)]^{1/2} \tag{3}$$

and

$$\bar{\bar{g}}(t)=\frac{1}{T}\int_{-T/2}^{T/2} g(t)\,\mathrm{d}t,$$

where g is some function of time and $T=5$ s.

u' and u'_R are fluctuating components of $\tilde{u}$ and $\tilde{u}_R$ derived by subtracting the short time means obtained by averaging over the 5-s periods of the correlation. Figure 12

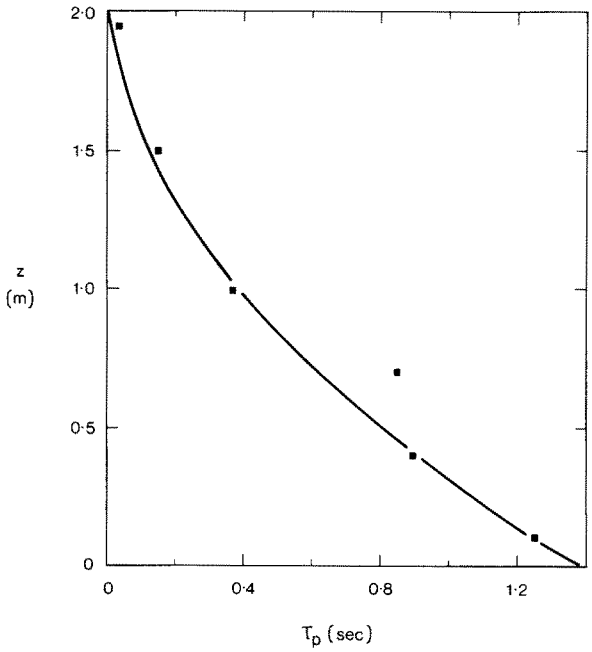

Fig. 11. Time delay, τ_p, of peak of R_{uu_R} *vs.* height, z, from R2.

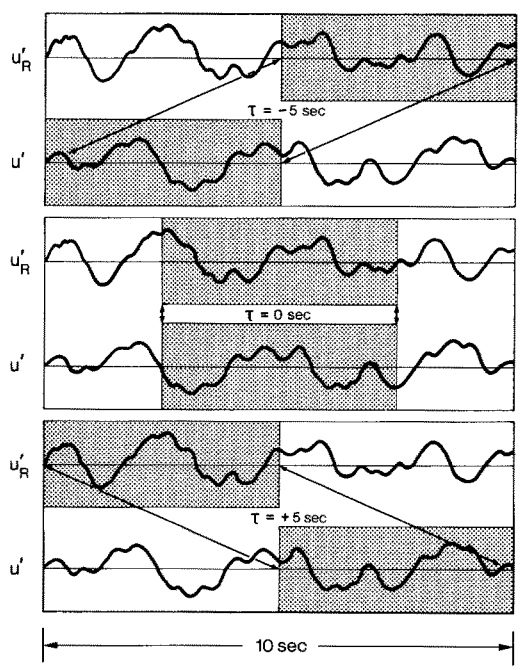

Fig. 12. Schematic relationship between 5-s intervals of u'_R and u' during formation of short period space-time correlations, $R^*_{uu_R}$.

presents a diagram of the relationship of the sections of the time traces in correspondence as τ changes.

A typical series of successive values of $R^*_{uu_R}$ is shown in Figure 13 for R2, $z = 1.0$ m. The immediately striking feature of the correlations is their strong periodicity; two periods are predominant, approximately 0.65 Hz, the stalk waving frequency, and 0.35 Hz, the average arrival frequency of gusts at the surface. Unlike their observed behaviour in normal rough-wall turbulent boundary layers, gusts tended to arrive over the waving wheat in trains of 3 or 4 with a well defined period, which appeared to scale upon U_R (see Part I).

To interpret the periodic behaviour of these short time correlations, it is useful to consider the result of correlating two harmonic signals, $\sin \omega_1 t$ and $\sin \omega_2 t$. It can be shown that, if

$$R^*(\tau) = \frac{1}{2T} \int_{-T}^{T} \sin \omega_1(t+\tau/2) \sin \omega_2(t-\tau/2)\, \mathrm{d}t,$$

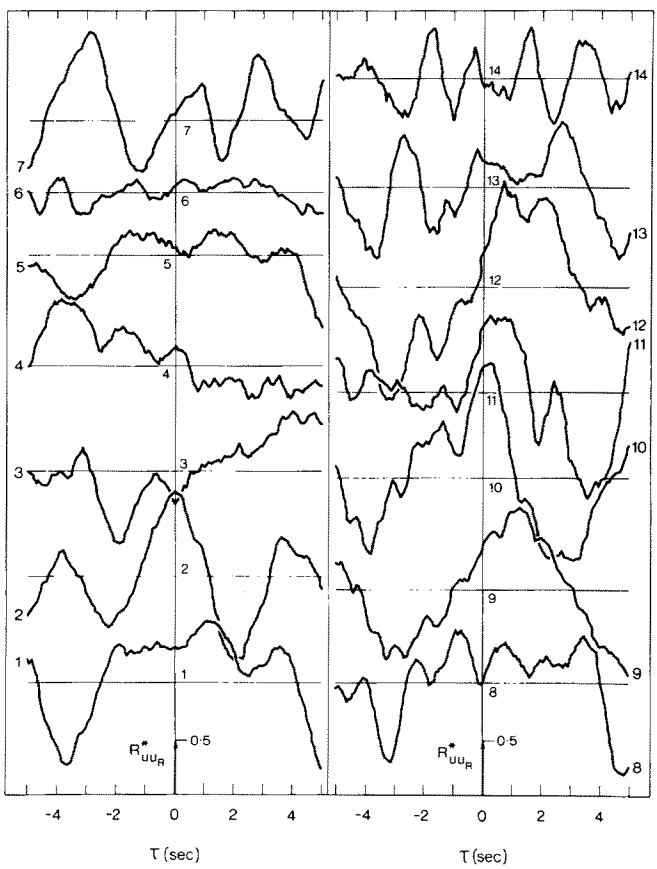

Fig. 13. Series of short period space-time correlations, $R^*_{uu_R}$, for successive 10-s intervals of R2; $z = 1.0$ m. Correlations are numbered consecutively.

then:

$$R^*(\tau) = \tfrac{1}{2}\{\cos(\omega_1+\omega_2)(\tau/2)\,\mathrm{sinc}\,[(\omega_1-\omega_2)T] - \\ -\cos(\omega_1-\omega_2)(\tau/2)\,\mathrm{sinc}\,[(\omega_1+\omega_2)T]\}, \tag{4}$$

where $\mathrm{sinc}\,(\psi) = \sin\psi/\psi$.

$R^*(\tau)$ therefore acts selectively to distinguish contributions from two signals with the same periodicity since sinc (0) = 1, but sinc (ψ) falls off rapidly with increasing ψ. If $\omega_1 = \omega_2 = \omega$, then $R(\tau) = \frac{1}{2}\cos\omega\tau - \mathrm{sinc}\,2\omega T$. If $\omega = 4.4$ rad/s (stalk waving frequency) and $T = 5$ s, sinc $2\omega T = 0.0158$, so that $R^*(\tau) \simeq \frac{1}{2}\cos\omega\tau$.

Bearing these results in mind, we can interpret the traces exhibiting strong periodicity at the waving or gust arrival frequency as times when, within one 10-s interval, velocity fluctuations at this frequency were present at both hot wires. In Figure 14 examples of $R^*_{uu_R}$ from the series of correlations from R2 at 1.0 m and 1.50 m are compared with the corresponding 10-s intervals of their time traces. The periodicity in the two signals which has been picked out by the correlations is obvious. The 'filtering' effect of R^* can be appreciated by comparing the smoothness of the R^* traces in Figure 14 with the time series from which they were derived. By counting the number of intervals when periodicity of one frequency or the other was dominant in the sequences of $R^*_{uu_R}$ for each height, Figure 15 was constructed; here the fraction of the total time when periodicity of one frequency was detected at both wires is plotted against height. Ten-second intervals when $R^*_{uu_R}$ was aperiodic or the frequency of the periodicity was equivocal were rejected, but occasionally both frequencies were clearly present. On average, 30% of the thirty 10-s traces for each height in the profile were rejected.

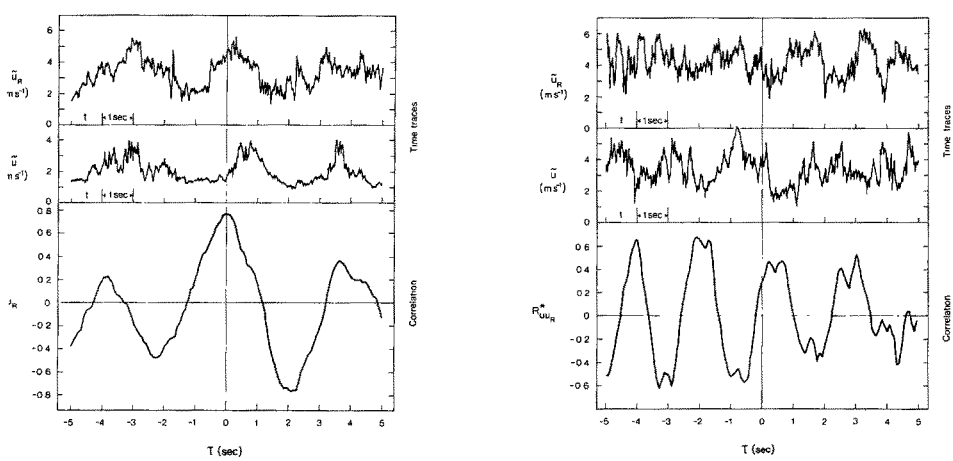

Fig. 14. Comparison of two short period space-time correlations with the corresponding 10-s time traces of $\tilde{u}$ and $\tilde{u}_R$ *vs.* time. From R2, (a) $z = 1.0$ m, (b) $z = 1.5$ m.

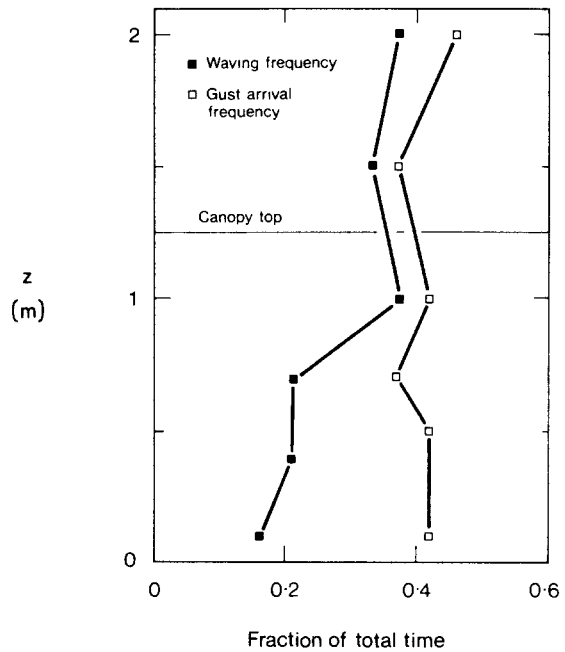

Fig. 15. Fraction of total time that periodic signal of same frequency was present in $\tilde{u}$ and $\tilde{u}_R$ *vs.* height.

We can see from Figure 15 that periodic gust arrival occupies about 40% of the total time irrespective of the position of the lower probe. The time occupied by waving frequency fluctuations, on the other hand, shows a definite decrease with height. This is partly a result of the observed shift to higher and lower frequencies of the wave motion impressed upon the air as it is convected from the centre of waving at the top of the stalks to higher and lower levels, respectively. As ω_1 and ω_2 move apart, $R^*(\tau)$ decreases in magnitude [see equation (4)]. It is apparent, however, that over a significant fraction of the total time, periodic velocity fluctuations can be discerned from a height of 2 m, through the canopy to the ground, and that a large fraction of the gusts arriving at 2 m are felt directly throughout the canopy.

3.4. Pressure velocity correlations

Because of technical problems, the pressure sensor, the strain-gauged wheat stalk bridges and the hot wires were only operated in conjunction during the two recorded points of R5. The power spectra of surface pressure and stalk displacement had peaks at precisely the same frequency, 0.7 Hz, while the waving-frequency velocity fluctuations, measured by the hot wires, showed a progressive decrease of frequency with height, the measured frequency just above the ground being only about 80% of its value at 1.0 m (see Part I). The pressure and velocity fluctuations are linked by Poisson's equation (see Burton, 1971) which in its integral form shows that pressure

fluctuations at a point are the result of velocity fluctuations over all space and need not be well correlated with those immediately nearby. The experimental results of Burton (1971), obtained in a rough-wall turbulent boundary layer, and the theoretical work of Mulhearn (1975), who calculated pressure-velocity correlations in a uniform shear flow using rapid distortion theory, both indicate that R_{pu} approaches zero at zero separation and time delay.

The long time pressure-velocity correlation, R_{pu}, from R5 at $z = 1.2$ m is presented in Figure 16. The trace is strongly periodic at the waving frequency. Although the 1.2-m correlation has contributions of longer time scales superimposed upon it, the dominant periodicity suggests that the waving motion is the prime inducer of surface pressure fluctuations. It was pointed out in Part I that the ratio of the r.m.s. pressure fluctuations to the shear stress, $(\overline{p^2})^{1/2}/\rho u_*^2$, at $z = 1.2$ m is about 4 times greater than that in any other rough-wall boundary layer available for comparison.

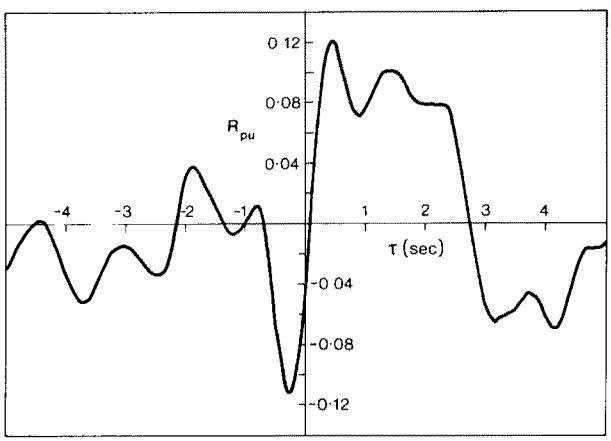

Fig. 16. Pressure velocity correlation coefficient, $R_{pu}(\tau)$, *vs.* time delay, τ, from R5; $z = 1.2$ m.

The periodicity of R_{pu} suggests that this 'extra pressure' might be a direct result of the coherent waving which would add to the correlation resulting from passage of large eddies and the random small-scale turbulence which must also be present.

Figure 17 presents the correlation between strain gauge output and velocity, R_{sgu}, for R5, $z = 1.2$ m. The correlation is strongly periodic, of course, since the stalk vibration is harmonic and well correlated with the neighbouring velocity. The maximum correlation corresponds to a time delay of 0.15 s, the stalks' motion slightly lagging the velocity fluctuations. The stalks which were strain-gauged were closely adjacent to the measuring station. The pressure strain-gauge correlation R_{psg}, of Figure 18 is purely periodic, a reflection of the stalks' behaviour in acting as a mechanical 'narrow band filter' for the velocity. The time delay of zero correlation is now the sum of the velocity-pressure and strain-gauge velocity time delays.

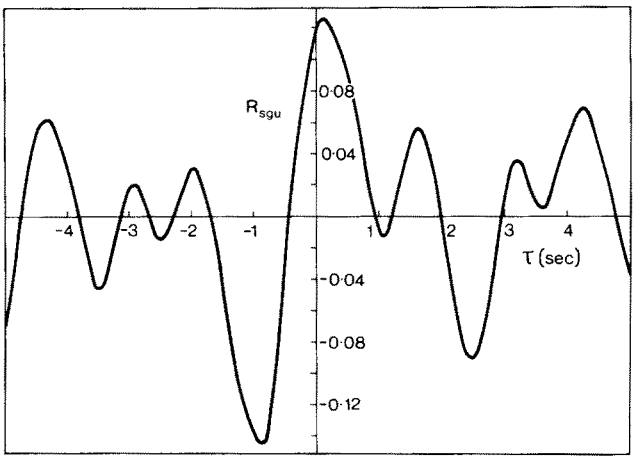

Fig. 17. Strain gauge output–pressure correlation, R_{sgu}, from R5; $z = 1.2$ m.

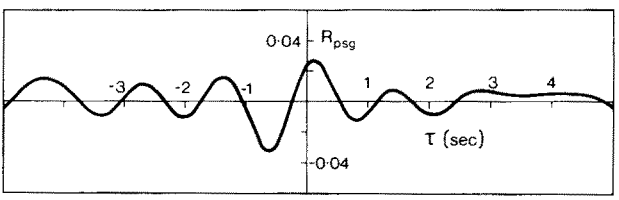

Fig. 18. Pressure–strain gauge correlation, R_{psg}, from R5; $z = 1.2$ m.

4. Conclusions

Examining the simultaneous time traces of streamwise velocity at a reference height of 2 m and at various heights above and within a wheat canopy suggested a direct connection between times of high reference velocity and periods of turbulence within the canopy. Conditional averaging of mean velocity and shear stress within the canopy revealed qualitatively different velocity and shear stress profiles during gusts and lulls. Strong winds penetrated much more effectively into the canopy. In the middle region of the canopy, the shear-stress contribution during a gust was an order-of-magnitude greater than when winds were low.

Decomposing the contributions to Reynolds stress into four quadrants and a 'hole' region, after the manner of Lu and Willmarth (1973), enabled the relative importance of different aspects of the velocity field in momentum transfer to be assessed. Within the middle regions of the crop, the resultant shear stress is largely the difference between gusts and outward interactions. This result is assumed to be caused by the wavelike particle path superimposed upon the turbulent fluid by

waving stalks in the aftermath of a gust. Above the canopy, bursts appeared to gain in importance and the relative magnitudes of the four quadrants appeared to approach the situation observed in a rough-wall channel flow by Nakagawa and Nezu (1977). The only comparable results in the atmosphere, those of Weiss and Allen (1976) over vine rows, confirm the predominance of gusts in momentum transfer close to the surface.

Space-time correlations of u_R and $u(z)$ allowed a definite vertical propagation velocity of maximum correlation to be derived. This velocity decreased as the lower wire entered the canopy, suggesting a progressive deceleration of the large eddies as they interact with the canopy.

It was realized that the long averaging period, 150 s, of the velocity correlations would obscure any intermittent features of the flow which might have a high correlation over a shorter time but which would be cancelled out by their random phase relationships in the course of a long average. Accordingly, successive short period space-time correlations were formed with time delays of ± 5 s in a 10-s interval. Many of these short time averages were observed to be periodic in time delay at the waving frequency or the average frequency of gust arrival. It can be shown that a short time average of the form defined in Equation (3) is a sensitive test of intervals when the two signals being correlated are periodic with the same frequency. It could be shown by counting the 10-s intervals when a certain frequency dominated the correlation, that for run R2, during 40% of the time, gusts were present in periodic trains penetrating the whole canopy and that velocity fluctuations caused directly by stalk waving were sensed by both wires for about 20% of the time when the lower wire was at the bottom of the canopy but for 40% of the time it was in the upper layers.

The pressure-velocity correlation, R_{pu}, has a strongly periodic appearance despite the long time average. The pressure fluctuations at the ground surface are apparently caused by the velocity fluctuations at the top of the canopy, and the coherent nature of the wavelike velocity fluctuations is assumed to account for a value of $(\overline{p^2})^{1/2}/\rho u_*^2$, about 4 times that observed in other rough-wall boundary layers.

Some of the conclusions presented here apply only to canopies where the stalks can wave coherently. Nevertheless, in less flexible canopies such as forests, we might still expect gusts to be the predominant mechanism of momentum transfer to the foliage. Features such as large instantaneous values of outward interaction would be absent however (as indeed they are in the results of Weiss and Allen over vine rows). Although the wave-like particle paths, imposed on the turbulent airflow, do not make a net contribution to momentum transfer, we might expect the increased mixing which they engender to be important in the transfer of the scalar species. During their vertical oscillations, fluid particles traverse regions of the canopy with significant temperature or scalar source-strength differences and, since such waves permeate the entire canopy for a significant fraction of the total time, we might expect the scalar transport to be increased significantly over the situation in a rigid canopy.

Acknowledgements

The author thanks Dr E. F. Bradley, Dr A. R. G. Lang, and Dr C. J. Barnes of this laboratory for helpful discussion and particularly Dr P. J. Mulhearn of the Royal Australian Naval Research Laboratory, Sydney, whose enthusiasm and guidance made this work possible.

References

Allen, L. H. Jr.: 1968, 'Turbulence and Wind Speed Spectra within a Japanese Larch Plantation', *J. Appl. Meteorol.* **7**, 73–78.

Brown, G. L. and Thomas, A. S. W.: 1976, *Large Structure in a Turbulent Boundary Layer*, Univ. of Adelaide, Dept. of Mech. Eng. Report TN16/76.

Burton, T. E.: 1971, *On the Generation of Wall Pressure Fluctuations for Turbulent Boundary Layers over Rough Walls*, Acoustics and Vibration Lab. Report No. 70208-4, Massachusetts Institute of Technology.

Corrsin, S.: 1974, 'Limitations of Gradient Transport Models in Random Walks and Turbulence', *Adv. Geophys.* **18A**, 25–59.

Cowan, I. R.: 1968, 'Mass, Heat and Momentum Exchange between Stands of Plants and their Atmospheric Environment', *Quart. J. Roy. Meteorol. Soc.* **94**, 523–544.

Dorman, C. E. and Mollo-Christensen, E.: 1973, 'Observation of the Structure on Moving Gust Patterns over a Water Surface ("Cat's Paws")', *J. Phys. Oceanogr.* **3**, 120–132.

Finnigan, J. J.: 1979, 'Turbulence in Waving Wheat. I. Mean Statistics and Honami', *Boundary-Layer Meteorol.* **16**, 181–211.

Grass, A. J.: 1971, 'Structural Features of Turbulent Flow over Smooth and Rough Boundaries', *J. Fluid Mech.* **50**, 233–255.

Hoerner, S. F.: 1965, *Fluid-dynamic Drag*, published by the author.

Inoue, K., Uchijima, Z., Horie, T., and Iwakiri, S.: 1975, 'Studies of Energy and Gas Exchange within Crop Canopies. (10) Structure of Turbulence in Rice Crop', *J. Agric. Meteorol. (Japan)* **31**, 71–82.

Isobe, S.: 1972, 'A Spectral Analysis of Turbulence in a Corn Canopy', *Bull. Nat. Inst. Agric. Sci. (Japan)* Ser. A, No. **19**, 101–112.

Laufer, J.: 1972, 'Recent Developments in Turbulent Boundary Layer Research', *1st Naz. Alta Mat., Symp. Math.* **9**, 299.

Lu, S. S. and Willmarth, W. W.: 1973, 'Measurements of the Structure of the Reynolds Stress in a Turbulent Boundary Layer', *J. Fluid Mech.* **60**, 481–511.

Maki, T.: 1975a, 'Interrelationships between Zero-plane Displacement, Aerodynamic Roughness Length and Plant Canopy Height', *J. Agric. Meteorol. (Japan)* **31**, 7–15.

Maki, T.: 1975b, 'Wind Profile Parameters of Various Canopies as Influenced by Wind Velocity and Stability', *J. Agric. Meteorol.* (Japan) **31**, 61–70.

Mulhearn, P. J.: 1975, 'On the Structure of Pressure Fluctuations in Turbulent Shear Flow', *J. Fluid Mech.* **71**, 801–813.

Nakagawa, H. and Nezu, I.: 1977, 'Prediction of the Contributions to the Reynolds Stress from Bursting Events in Open Channel Flows', *J. Fluid Mech.* **80**, 99–128.

Seginer, I. and Mulhearn, P. J.: 1978, 'A Note on Vertical Coherence of Streamwise Turbulence inside and above a Model Plant Canopy', *Boundary-Layer Meteorol.*, **14**, 515–523.

Shaw, R. H.: 1977, 'Secondary Wind Speed Maxima Inside Plant Canopies', *J. Appl. Meteorol.* **16**, 514–521.

Tan, H. S. and Ling, S. C.: 1961, *A Study of Atmospheric Turbulence and Canopy Flow*, Therm Advanced Research Division, Report No. TAR-TR 611, Ithaca, New York.

Thom, A. S.: 1972, 'Momentum, Mass and Heat Exchange of Vegetation', *Quart. J. Roy. Meteorol. Soc.* **98**, 124–134.

Townsend, A. A.: 1976, *The Structure of Turbulent Shear Flow*. Cambridge Univ. Press.

Weiss, A. and Allen, L. H. Jr.: 1976, 'The Flux-angle Distribution of Momentum as Determined from Propellor Anemometer Measurements', *Quart. J. Roy. Meteorol. Soc.* **102**, 775–779.
Willmarth, W. W.: 1975, 'Structure of Turbulence in Boundary Layers', in Yih, C.-S. (ed.), *Adv. Appl. Mech.*, **15**, Academic Press, New York, pp. 159–254.